Catalysis Science & Technology

ROYAL SOCIETY OF CHEMISTRY

PAPER

View Article Online
View Journal | View Issue

Cite this: *Catal. Sci. Technol.*, 2020, 10, 2378

Integrated adsorption and photocatalytic degradation of VOCs using a TiO_2/diatomite composite: effects of relative humidity and reaction atmosphere

Guangxin Zhang, *[abc] Arman Peyravi,[c] Zaher Hashisho, *[c] Zhiming Sun,*[b] Yangyu Liu,[b] Shuilin Zheng[b] and Lexuan Zhong [d]

Received 26th January 2020,
Accepted 21st March 2020

DOI: 10.1039/d0cy00168f

rsc.li/catalysis

In this study, the adsorption and photocatalytic degradation performances of a TiO_2/diatomite composite were investigated using ketones and alcohols with different carbon chain lengths as target pollutants. The effects of relative humidity and oxygen on the photocatalytic process of the composite and the different roles of water vapor and oxygen in this process were investigated. The adsorption capacity of VOCs over the composite decreased exponentially with the increase of relative humidity. During the degradation of the ketones and alcohols using the composite, the optimal relative humidity condition for VOC degradation was related to the length of the carbon chain. The optimal relative humidity for acetone, 2-butanone, and 2-heptanone degradation was 5%, 15%, and 30%, respectively. For the tested alcohols, the optimal relative humidity for degradation of isopropanol, isobutanol, and 1-heptanol was 5%, 15%, and 50%, respectively. When dry air was used, a high VOC degradation rate was observed. However, at the optimum relative humidity but in the absence of oxygen, VOC degradation hardly occurred. Compared with water vapor, oxygen played a more important role in the photocatalytic degradation of ketones and alcohols by the TiO_2/diatomite composite.

1. Introduction

VOCs are common pollutants that are released from many decoration materials and industrial products.[1,2] The harmful effects of VOCs have induced the development of various abatement techniques (destruction methods, capture methods, and hybrid methods) and materials.[3,4] Among them, adsorption and advanced oxidation are efficient and environmentally friendly methods. The combination of adsorption and photocatalysis is also an active research topic. Herein, the synthesis of photocatalysts is related to the selection of a matrix with excellent adsorption ability. Carbon materials,[5–7] molecular sieves,[8–10] and metal–organic framework compounds[11,12] have been used as photocatalyst supporters. Pham *et al.*[13] used porous polyurethane as a substrate supporting V-doped TiO_2 to increase the adsorption ability of the photocatalyst for the removal of toluene. Activated carbon fiber felt was also used as a carrier to prepare porous TiO_2/activated carbon fiber felt porous composites for toluene removal.[14] Lyu *et al.*[15] prepared a microporous homojunction–adsorption layer on TiO_2 to enhance the adsorption and improve the photocatalytic mineralization of toluene. The integration of adsorption and photocatalytic degradation endowed the materials with excellent performances.

Natural porous minerals have been used for VOC adsorption because of their porous structure and stability.[16–18] In addition, porous minerals have served as supports to be used in the preparation of photocatalysts.[19–21] Chen *et al.*[22,23] prepared a nitrogen-doped TiO_2/diatomite granule catalyst for the degradation of tetracycline hydrochloride. Li *et al.*[24] found that fluorine doping could induce the creation of oxygen vacancies in TiO_2/diatomite. Sun *et al.*[25] adopted a method for constructing a g-C_3N_4/TiO_2 hybrid over diatomite to enhance the visible light performance of TiO_2/diatomite. However, most of the research studies focused on the degradation of liquid pollutants. We assumed that the purification of gas phase pollutants could explore the application of this class of materials. Our group had previously prepared a nano-TiO_2/

[a] *School of Materials Science and Engineering, Shandong University of Science and Technology, Qingdao 266590, PR China. E-mail: gxzhang2019@sdust.edu.cn*
[b] *School of Chemical and Environmental Engineering, China University of Mining & Technology (Beijing), Beijing 100083, PR China. E-mail: zhimingsun@cumtb.edu.cn*
[c] *Department of Civil and Environmental Engineering, University of Alberta, Edmonton, AB T6G 2W2, Canada. E-mail: hashisho@ualberta.ca*
[d] *Department of Mechanical Engineering, University of Alberta, Edmonton, AB T6G 1H9, Canada*

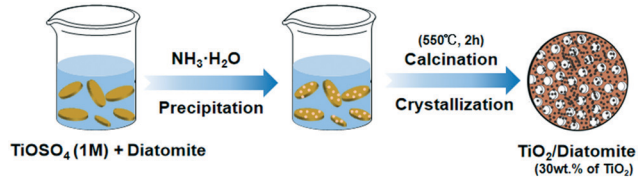

Fig. 1 Illustration of the preparation of the TiO_2/diatomite composite.

diatomite composite for dealing with formaldehyde.[26] The introduction of diatomite provided the composite with outstanding photocatalytic activity because of the strong formaldehyde adsorption capacity and the good dispersion of TiO_2 nanoparticles. The principal component of diatomite is amorphous silica or silicate, which is stable in structure and chemical properties and recyclable. Porous minerals such as

Table 1 Characteristic information of the TiO_2/diatomite composite

Photocatalyst	BET surface area (m^2 g^{-1})	Total pore volume (cm^3 g^{-1})	Average pore size (nm)	TiO_2 crystallite size (nm)
TiO_2/diatomite	40.0	0.078	6.0	10.9

Table 2 Physicochemical properties of VOCs

VOC	Category	Molecular formula	Boiling point (°C)	Dipole moment[a] (D)	Supplier
Acetone	Ketone	C_3H_6O	57	2.88	Fisher Bioreagents
MEK		C_4H_8O	80	2.78	Fisher chemical
2-Heptanone		$C_7H_{14}O$	151	2.61	Sigma-Aldrich
Isopropanol	Alcohol	C_3H_8O	82	1.58	Fisher scientific
Isobutanol		$C_4H_{10}O$	117	1.64	Fisher chemical
1-Heptanol		$C_7H_{16}O$	176	1.73	Acros organics

[a] Data from Lange's Handbook of Chemistry, Seventeenth Edition.

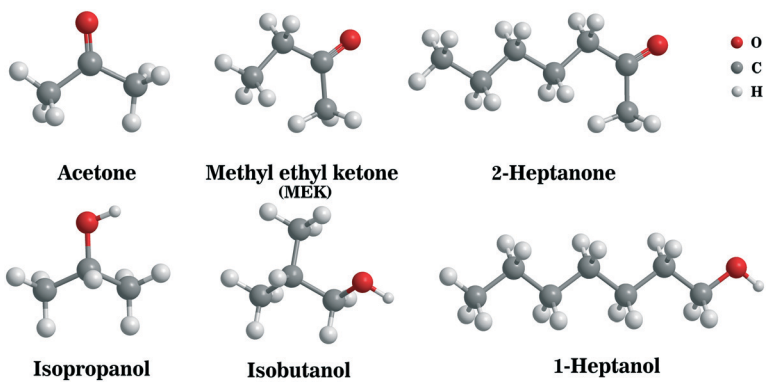

Fig. 2 Molecular structure models of VOCs.

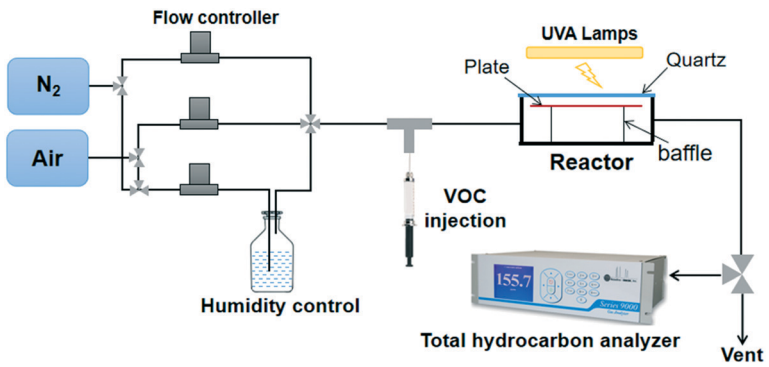

Fig. 3 Schematic diagram of the adsorption and photocatalytic degradation setup.

diatomite can provide special physicochemical adsorption or microchemical reaction sites which give them excellent adsorption and capture functions. The support of TiO_2 nanoparticles by minerals can significantly enhance the adsorption property of the catalyst and provide more active sites for the degradation of pollutants.

In the photocatalytic degradation process, many factors could have effects on the degradation process.[27–30] Oxygen and water vapor were found to play extremely important roles in photocatalytic oxidation. Oxygen easily combines with electrons to generate superoxide radicals; water facilely reacts with holes to generate hydroxyl radicals. These two strong oxidizing radicals react with VOCs, and finally, degrade VOC molecules into carbon dioxide and water. In previous studies, researchers reported that the competitive adsorption between water vapor and VOC molecules on the photocatalyst surface affected the photocatalytic degradation of VOCs.[31] Besides, some literature reports stated that the hydroxyl radicals produced in the photoreaction mainly came from the water adsorbed on the surface of the photocatalyst.[32,33] Mo *et al.*[34] found that the water level had an obvious effect on toluene photocatalytic decomposition and by-product generation. Their research indicated that: the by-products produced during photocatalytic degradation had a shorter residence time and faster release rate on the surface of the photocatalyst at high water concentration; higher decomposition efficiency and lower by-product generation were acquired at low water concentration; deactivation of the photocatalyst occurred when the water vapor level approached 0. Sleiman *et al.*[35] also found that the relative humidity was a critical factor in the reaction processes. Their research indicated that high mineralization extent could be obtained through direct hole oxidation at low RH. The mineralization rate was low involving hydroxylation by OH radicals at high RH. However, most of the papers reported that the effects of water vapor and reaction atmosphere on the photocatalytic abilities of materials were just for one pollutant. It is assumed that VOCs with different structures may be affected to different degrees under different degradation conditions. To our knowledge, the influence of the VOC carbon chain length on the adsorption and photocatalytic process has not been reported.

The purpose of this work was to study the adsorption and photocatalytic activity of a nano-TiO_2/diatomite composite for

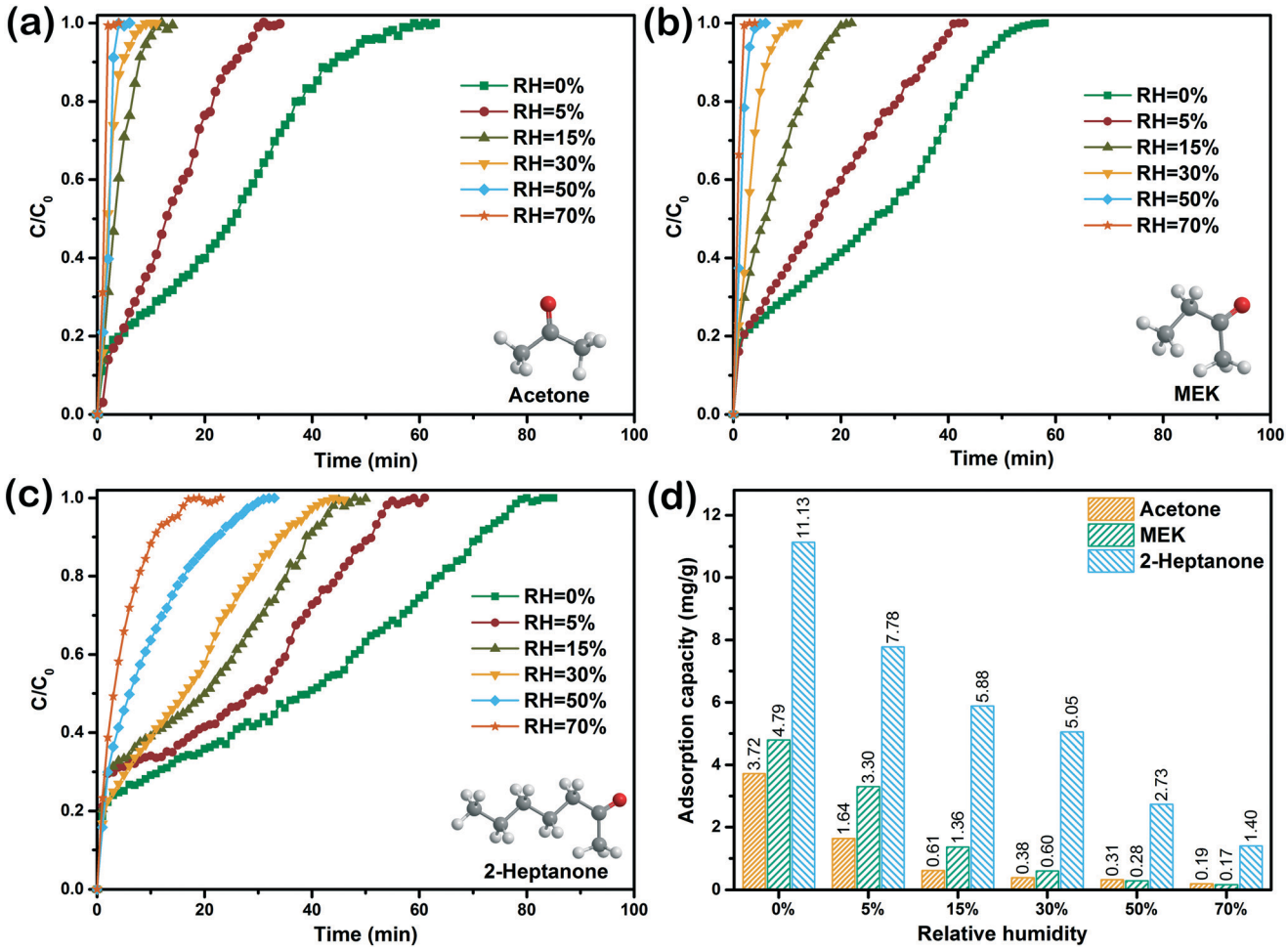

Fig. 4 Effect of relative humidity on the adsorption of ketones by the composite: (a) acetone, (b) MEK, and (c) 2-heptanone, and (d) adsorption capacity.

VOC degradation at different concentrations of water vapor and oxygen. Using three alcohols and three ketones as target pollutants, this work explores the relationship of suitable humidity conditions to degradation of VOCs with different carbon chain lengths.

2. Experimental

2.1. Materials

Three alcohols (isopropanol, isobutanol, and 1-heptanol) and three ketones (acetone, methyl ethyl ketone, and 2-heptanone) were used as VOCs in this work. All chemicals were of analytical grade and used without further treatment. The nano-TiO_2/diatomite composite was used as a photocatalyst in this work. The detailed preparation and characterization results of this composite were described in our previous work[26] and are briefly reviewed here. The preparation process of this composite is shown in Fig. 1. The preparation process mainly included two steps (hydrolysis precipitation and calcination crystallization). Briefly, a certain quantity of diatomite was mixed with 1 M titanyl sulfate solution in a beaker. Dilute ammonia was adopted to adjust the solution pH to 4.5. The precipitate was filtered and dried, and then the sample was calcined at 550 °C for 2 h in a muffle furnace. The calcined product was the TiO_2/diatomite composite. The basic characteristic information of the TiO_2/diatomite composite is listed in Table 1. The physicochemical properties and molecular structures of the alcohols and ketones are shown in Table 2 and Fig. 2, respectively.

2.2. Adsorption and photocatalytic degradation experiments

In this study, a dynamic adsorption–photocatalytic degradation setup was used to determine the adsorption–photocatalytic degradation performance for the VOCs, as shown in Fig. 3. The setup consisted of a VOC generating system, a reactor, a humidity and atmosphere regulating system, and a VOC detecting system. The VOC generation system consisted of a syringe pump (Fusion 100, Chemyx Inc.) which injected the liquid VOC into a dry air stream to generate a certain concentration (10 ppm) of the VOC. The air stream (1 L min^{-1}) was regulated by a mass flow controller (Alicat Scientific). The reactor was a rectangular aluminum enclosure (0.13 L) containing the photocatalyst and equipped

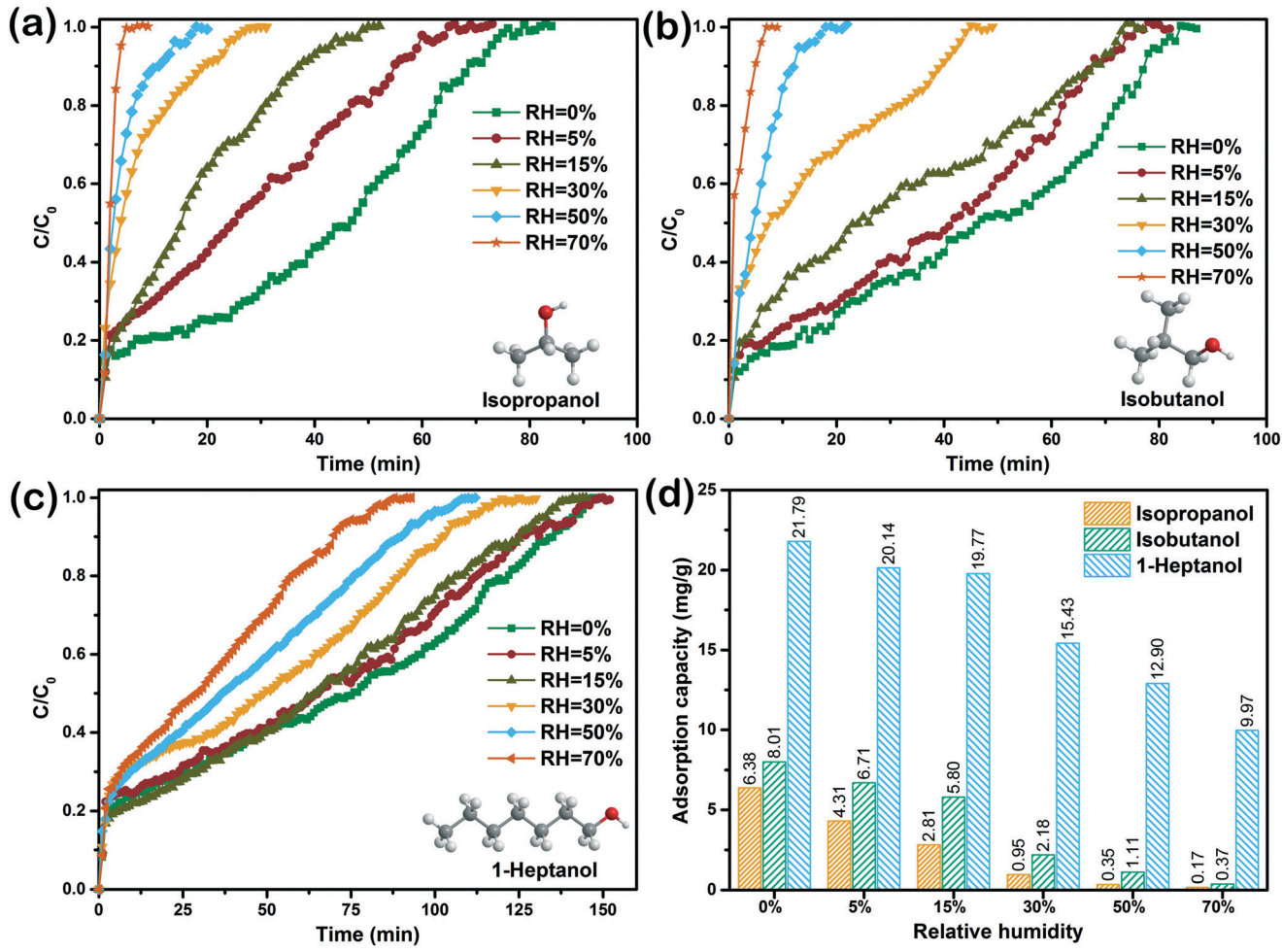

Fig. 5 Effect of relative humidity on the adsorption of alcohols by the composite: (a) isopropanol, (b) isobutanol, and (c) 1-heptanol, and (d) adsorption capacity.

with two UVA lamps (T5-JL, Shanghai Shenzhen light electric appliance). The reactor was gas-tight and equipped with a removable quartz window. The slurry was prepared by mixing 0.15 g of powder TiO_2/diatomite with water, followed by ultrasonication to disperse the powder. The slurry was coated on an aluminum substrate (104 mm × 83 mm) with a film thickness of 0.1 mm. After oven drying of 30 min, the aluminum plate was put in the reactor and sealed by a quartz plate. The plate was located at 5.5 mm below the bottom of the quartz plate. The plate was supported by two baffles which also helped in directing the flow. The reactor was illuminated by two UVA lamps (8 W). The light intensity on the surface of the plate was 0.78 mW cm^{-2} measured by a UVX radiometer (Ultra-Violet Products Ltd. USA). The humidity and atmosphere regulating system controlled the relative humidity of the air stream by mixing dry air with humid air (obtained using a water bubbler). The system was also used to control the oxygen content of the VOC laden stream by changing the ratio of nitrogen to air. The VOC laden stream passed through the reactor, and a total hydrocarbon analyzer (Series 9000, Baseline Mocon) measured the VOC concentration at the outlet of the reactor in real-time. When the experiment began, the VOC laden stream with a certain relative humidity and oxygen level passed through the whole system. In the adsorption process, the reactor was shaded with a cover to keep the dark condition. When the adsorption curves indicated that the adsorption saturation was reached, the lamps were turned on to provide light for the photocatalytic process.

In this work, the total organic carbon content was used to characterize the VOC concentration. The VOC adsorption capacity was calculated using the following formula:

$$Q = \sum_{0}^{t} \frac{F(C_{in} - C_{out})}{m} \Delta t$$

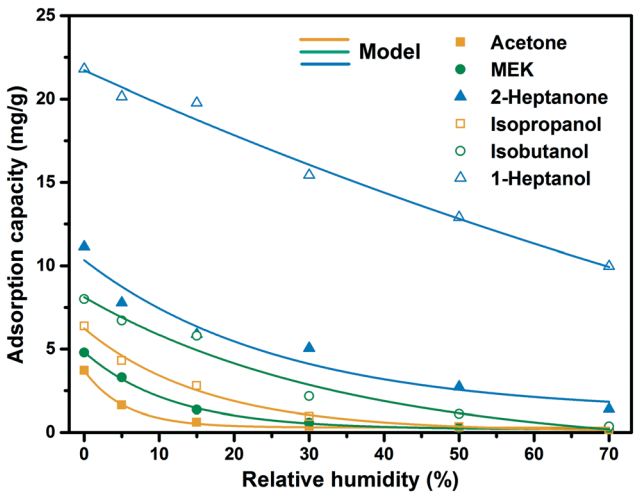

Fig. 6 Experimental results and model of the adsorption capacities of VOCs under different relative humidity conditions.

Table 3 Fitting parameters of the exponential model

VOC	A	B	y_0	R^2
Acetone	3.404	−0.181	0.304	0.996
MEK	4.634	−0.086	0.191	0.998
2-Heptanone	9.143	−0.038	1.201	0.922
Isopropanol	6.175	−0.061	0.071	0.989
Isobutanol	9.198	−0.028	−1.076	0.958
1-Heptanol	34.433	−0.006	−12.713	0.973

where Q is the adsorption capacity (mg g^{-1}), F is the gas flow rate (1 L min^{-1}), C_{in} and C_{out} are the gas concentration at the inlet and outlet of the reactor (mg cm^{-3}), respectively, m is the mass of the catalyst (g), and t is the adsorption time (min).

The degradation rate of the VOCs was calculated based on the change of total organic carbon content, as shown in the following equation:

$$D = \frac{C_{in} - C_{out}}{C_{in}} \times 100\%$$

where D is the total organic carbon degradation rate, and C_{in} and C_{out} are the total organic carbon concentration (ppm) at the inlet and outlet of the reactor, respectively.

3. Results and discussion

3.1. Effect of water vapor

In this section, the influence of water vapor concentration on the adsorption and degradation performances of the TiO_2/diatomite composite for VOCs with different carbon chain lengths was investigated by changing the environmental relative humidity in the reactor. The relative humidity (RH) was set to 0, 5%, 15%, 30%, 50%, and 70%, respectively, and the flowing gas was air (oxygen content was 21%).

Fig. 4 shows the adsorption breakthrough curves and adsorption capacities of the nano-TiO_2/diatomite composite for acetone, MEK and 2-heptanone under different relative humidity conditions. The adsorption breakthrough curves of the three ketones showed a similar trend. At the initial adsorption time, the outlet concentration increased rapidly, indicating immediate breakthrough. When the VOC entered the reactor, the baffle steered the VOC flow onto the surface of the plate, making a close contact between the VOC and the photocatalyst coating on the plate. Because the adsorption was a dynamic adsorption process, some VOC molecules would pass through the adsorption space quickly. The VOC concentration increased to a certain point rapidly and then the relatively slow adsorption process started along with the dramatic increase of VOC molecules at the outlet of the reactor. When the outlet VOC concentration was equal to the inlet VOC concentration, the adsorption reached saturation on the surface of the composite. Obviously, when the relative humidity was 0, that was for dry air, the adsorption breakthrough curves of the three ketones showed the longest

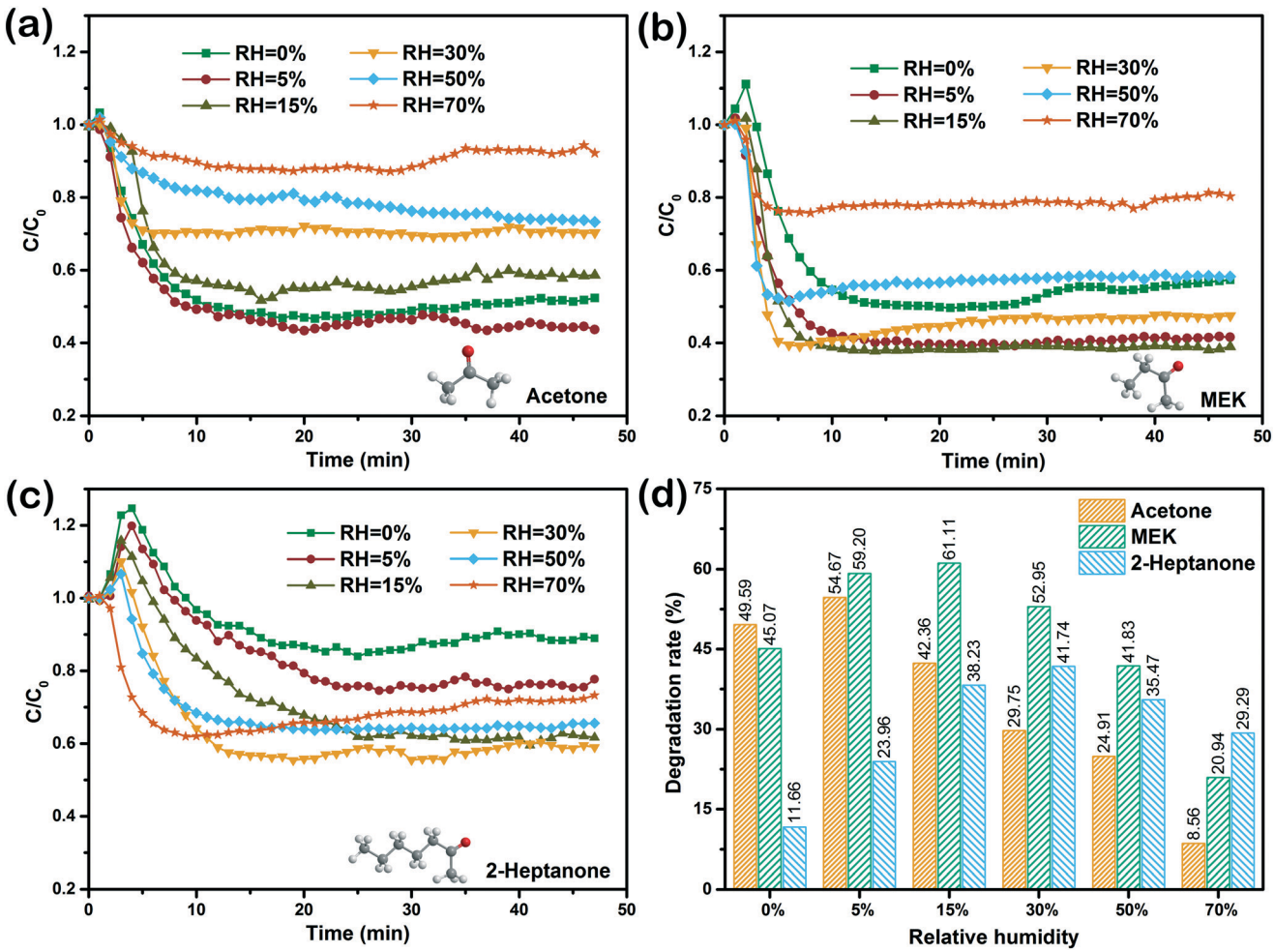

Fig. 7 Effect of relative humidity on the degradation of ketones by the composite: (a) acetone, (b) MEK, and (c) 2-heptanone, and (d) degradation rate.

adsorption time. By comparing the adsorption breakthrough curves of the composite under different relative humidity conditions, it can be seen that the relative humidity had an influence on the adsorption process. With the gradual increase in relative humidity, the water content in the gas increased accordingly. Therefore, water molecules competed with VOC molecules for adsorption on the surface of the composite, resulting in fewer adsorption sites on the surface of the composite available for VOC adsorption, and a shorter adsorption time was required for the composite to reach adsorption saturation.[36] Another reason is that the water layers caused by the hydrogen bonds of water molecules with surface hydroxyls of the composite weakened the adsorption forces between the VOC and composite.[37,38] Accordingly, the adsorption breakthrough curves of the three ketones shifted to the left, indicating the shorter time for adsorption saturation with increasing relative humidity. It can be also seen from Fig. 4 that, under the same relative humidity, the VOC with a long carbon chain had a higher adsorption capacity on the composite compared to the VOC with a short carbon chain. This may be related to the boiling point of VOC molecules. The higher the boiling point, the stronger the intermolecular forces of VOC molecules, and the more likely the VOC molecules were accumulated over the active sites of the composite. 2-Heptanone had the highest boiling point, resulting in the highest adsorption capacity among the three ketones. Fig. 4(d) shows the adsorption capacity of acetone, MEK and 2-heptanone on the composite under different relative humidity conditions. It can be clearly seen that the adsorption capacities of the three ketones in the composite decreased gradually with the increase of relative humidity.

Fig. 5 shows the adsorption breakthrough curves and adsorption capacities of the nano-TiO_2/diatomite composite for isopropanol, isobutanol, and 1-heptanol under different relative humidity conditions. With the gradual increase of relative humidity, the adsorption time required for the adsorption saturation of the composite decreased. This trend was similar to that of the above mentioned relative humidity for ketones. As can be seen from Fig. 5(d), the adsorption capacities of the three alcohols on the composite decreased gradually with the increase of relative humidity. Also,

1-heptanol with the highest boiling point showed the highest adsorption capacity among the three alcohols.

In order to clearly compare the adsorption performances of the ketones and alcohols on the composite, Fig. 6 summarizes the adsorption capacity under different relative humidity conditions for each compound. Under the same humidity, the adsorption capacity of the VOCs followed the order: 1-heptanol > 2-heptanone > isobutanol > isopropanol > MEK > acetone. The order was related to the different boiling points of the six VOCs. The VOC with a high boiling point had a high adsorption capacity. Fig. 6 also shows the negative dependence of adsorption capacity on relative humidity. This dependence of adsorption capacity on relative humidity can be fitted with an exponential decay function expressed by the following:

$$y = y_0 + Ae^{Bx}$$

where y is the adsorption capacity (mg g^{-1}), and x is the relative humidity (%). A, B and y_0 are the fitting parameters of the equation. The exponential fitting results are shown in Table 3. The high R^2 values indicated that the exponential model was in good agreement with the experimental data, and confirmed the negative exponential dependence of adsorption capacity on relative humidity. An interesting phenomenon was that the absolute values of parameter B for the ketones were higher than those for the alcohols. This may be related to the stronger polarity of ketones than that of alcohols, which induced the strong interaction force between the ketones and water vapor. Therefore, the ketones were more susceptible to relative humidity than the alcohols overall.

The results described above were obtained in the absence of UVA light. When the composite was irradiated with UVA light, VOC degradation occurred. Fig. 7 shows the degradation curves and degradation rates of the three ketones, under different relative humidity conditions, over the TiO_2/diatomite composite when UVA light was turned on. The degradation curves of the three ketones were slightly different in the initial stage of degradation. At the beginning of the degradation curves of MEK and 2-heptanone, the total organic carbon concentration at the outlet of the reactor

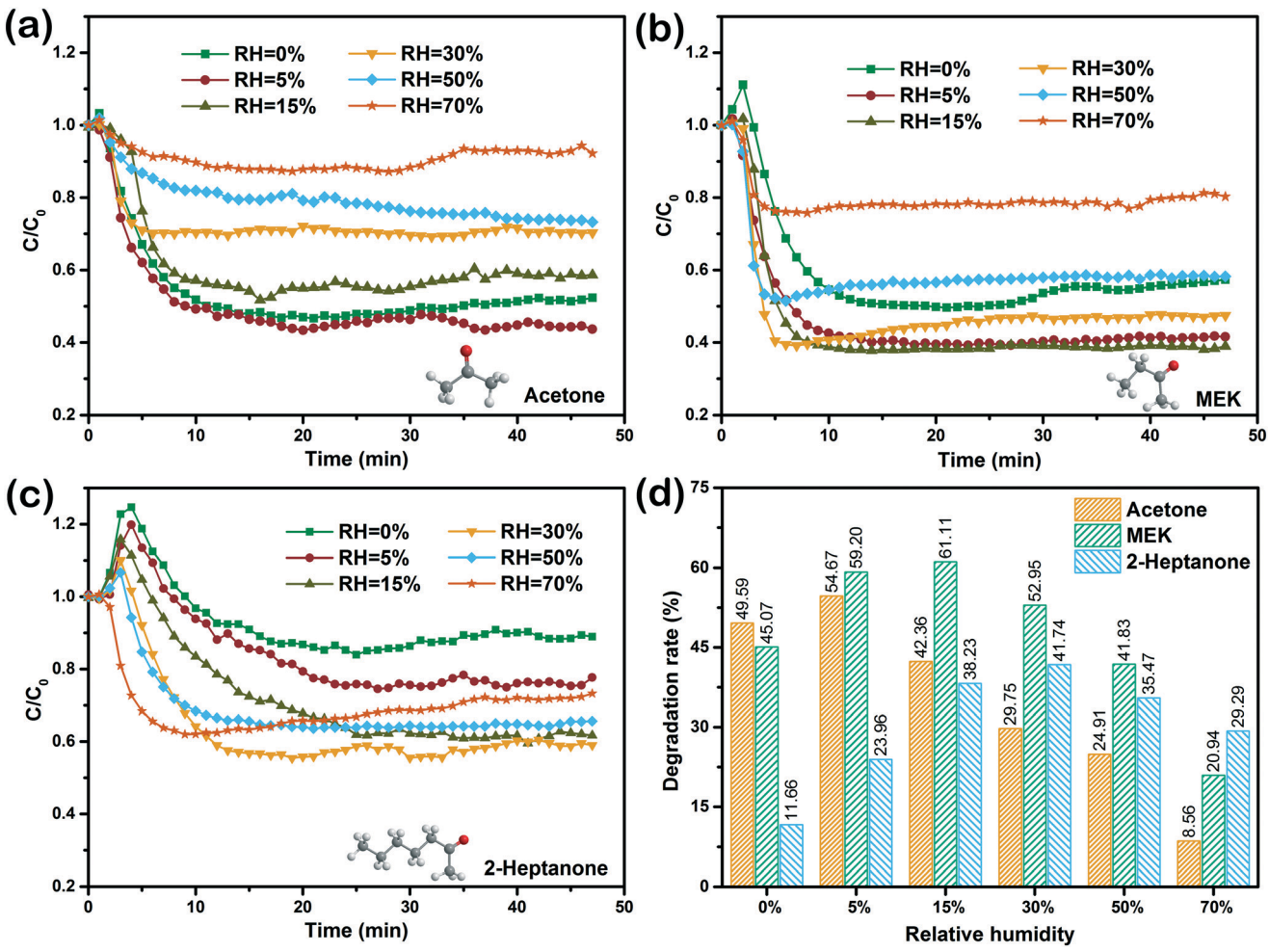

Fig. 8 Effect of relative humidity on the degradation of alcohols by the composite: (a) isopropanol, (b) isobutanol, and (c) 1-heptanol, and (d) degradation rate.

increased to some extent. One reason was that when UVA light was turned on, the surface temperature of the composite rose, which caused the VOC adsorbed by the composite to be desorbed. Another reason was that the VOC molecules adsorbed on the surface of the composite were degraded, and intermediate products were generated. Some intermediate products were purged out of the reactor by the incoming VOC. The above two reasons caused the total organic carbon concentration at the outlet of the reactor to rise in the preliminary stage. After a period of UVA illumination, the total organic carbon content declined rapidly and then stabilized. The steady state total organic carbon content (within 20 min before the end of illumination) was selected to calculate the degradation rate of total organic carbon, and the results are shown in Fig. 7(d). The optimal relative humidity was obtained when the total organic carbon degradation rate was the highest. The optimal relative humidity for acetone was 5%, MEK 15%, and 2-heptanone 30%. Obviously, with the increase of the carbon chain length of the ketone, the optimal relative humidity in the photocatalytic degradation process also increased, which may be because the long VOC carbon chain made the photocatalytic degradation process complex, and more water molecules were required, leading to a higher optimal relative humidity in the photocatalytic degradation process. In addition, the VOC with a longer carbon chain had the higher adsorption capacity under the low relative humidity, which indicated that more VOC molecules accumulated over the active sites. The degradation process could not happen sufficiently, resulting in the low degradation efficiency.

Fig. 8 shows the degradation curves and degradation rates of the nano-TiO_2/diatomite composite for the three alcohols under different relative humidity conditions. Unlike the degradation process of the ketones, the elevated outlet levels of total organic carbon were more apparent in the initial stages of alcohol degradation. The reason may be that the intermediate products generated in the initial degradation process had weak forces with the composite. The intermediate products that were not easily adsorbed by the composite were purged out of the reactor together with the continuous inflow of VOC gas.

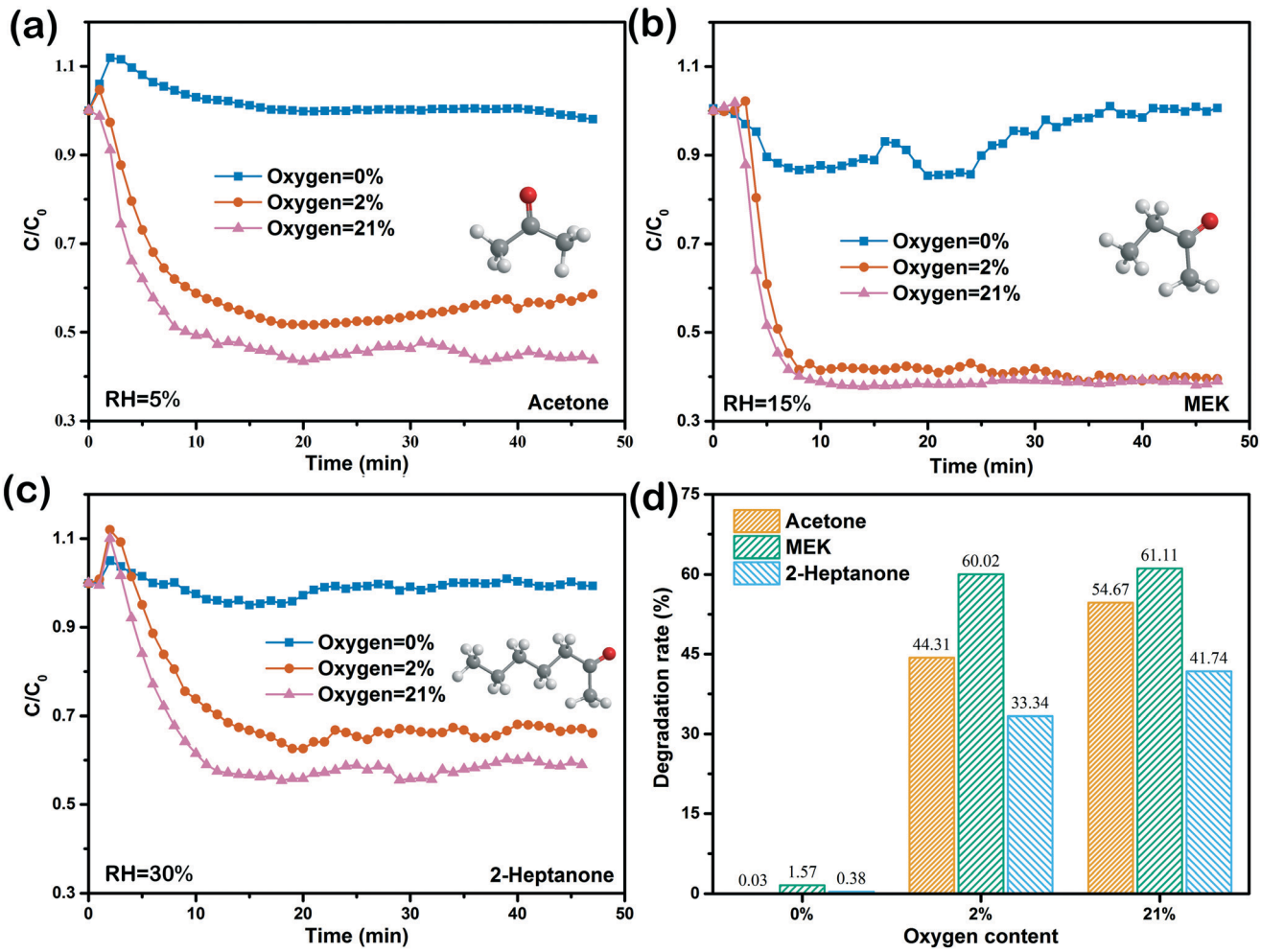

Fig. 9 Effect of oxygen concentration on the degradation of ketones by the composite: (a) acetone, (b) MEK, and (c) 2-heptanone, and (d) degradation rate.

After a short period of illumination, the intermediate products produced by photocatalysis began to be gradually degraded, and the total organic carbon content at the outlet of the reactor began to decrease. When VOC adsorption and degradation reached equilibrium, the total organic carbon content stabilized at a certain level. The steady state total organic carbon content within 20 min before the end of illumination was used to calculate the degradation rate of the total organic carbon (Fig. 8(d)). The total organic carbon degradation rate in the degradation process of isopropanol was the highest when the relative humidity was 5%. The optimal relative humidity for isobutanol and 1-heptanol was 15% and 50%, respectively. Notably, with the increase of the carbon chain length of alcohols, the appropriate relative humidity in the photocatalytic degradation process also increased. These results were similar to the degradation of the ketones under different relative humidity conditions, which means that the optimal VOCs with different carbon chain lengths have a certain relationship with the relative humidity.

3.2. Effect of reaction atmosphere

In this study, the oxygen content was set to 0, 2%, and 21% by changing the ratio of air and nitrogen. The optimum relative humidity for the degradation of each VOC, as found in section 3.1, was used. The relative humidity of acetone, MEK and 2-heptanone was 5%, 15%, and 30%, respectively, and that of isopropanol, isobutanol and 1-heptanol was 5%, 15%, and 50%, respectively.

Fig. 9 shows the degradation curves and degradation rates of the nano-TiO_2/diatomite composite for acetone, MEK and 2-heptanone under different oxygen contents. According to the degradation data, when the oxygen content was 0, almost no photocatalytic degradation reaction occurred for the three ketones. When the oxygen content increased to 2%, the total organic carbon degradation rate of the three ketones was considerably increased. When the oxygen content was 21%, the degradation rate was slightly higher than that when the oxygen content was 2%. The experimental results showed that oxygen played an important role in

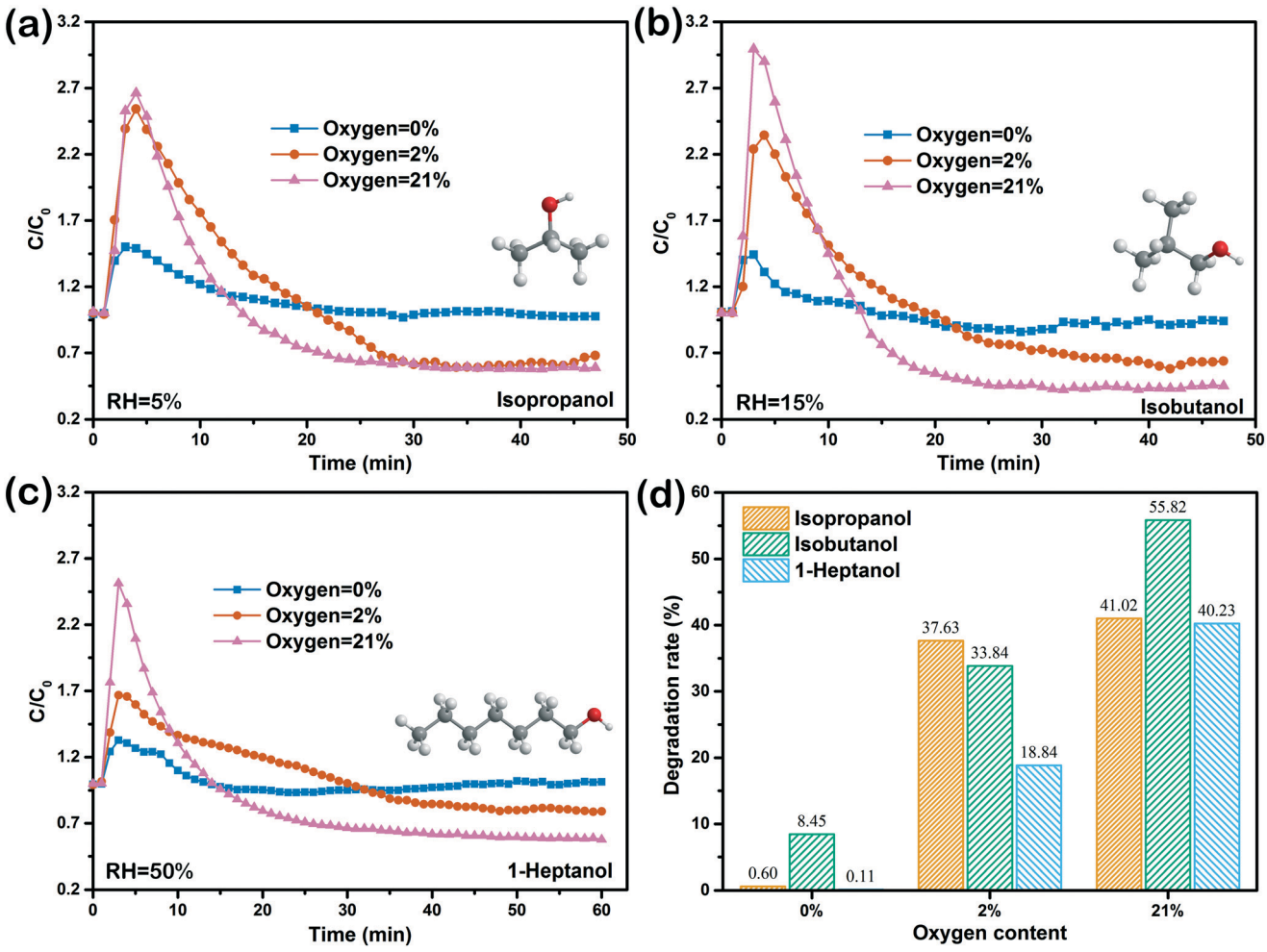

Fig. 10 Effect of oxygen concentration on the degradation of alcohols by the composite: (a) isopropanol, (b) isobutanol, and (c) 1-heptanol, and (d) degradation rate.

the photocatalytic degradation of the ketone organic compounds by the composite, and the VOCs basically did not undergo a degradation reaction in the absence of oxygen.

Fig. 10 shows the degradation curves and degradation rates of the nano-TiO_2/diatomite composite for isopropanol, isobutanol, and 1-heptanol under different oxygen contents. The experimental results were similar to the degradation of the three ketones by the composite under different oxygen contents. When the oxygen content was 0%, no considerable degradation of the three alcohols was observed, and when the oxygen content was increased to 2%, the VOCs degraded obviously. Photocatalytic degradations of ketones and alcohols under different oxygen contents showed that oxygen played an important role in VOC photocatalytic degradation. Compared to photocatalytic degradation results under different relative humidity conditions, the VOC degradation reaction still occurred when the relative humidity was 0. This may be because the dry air used in this work still had an extremely low water vapor. Therefore, water reacted with photogenerated holes to generate hydroxyl radicals. Meanwhile, the superoxide radicals may also be produced from oxygen. Hydroxyl radicals and superoxide radicals were involved in the degradation of the VOCs. However, VOC degradation did not happen when the oxygen level was 0. This may be explained by the fact that: in the photocatalytic process, oxygen was reduced by photogenerated electrons to superoxide radicals, and superoxide radicals could react with electrons to produce hydrogen peroxide, and then hydroxyl radicals can be produced from the reaction of hydrogen peroxide with superoxide radicals.[39–41] This result indicated that oxygen was an essential factor in photocatalytic degradation of VOCs over TiO_2/diatomite.

4. Conclusions

Three ketones and three alcohols were used as VOCs for investigating the effects of water vapor and reaction atmosphere on the adsorption and degradation of VOCs. For the VOC adsorption process of the nano-TiO_2/diatomite composite, the adsorption capacity had negative exponential dependence on the relative humidity. In the degradation process of the ketone and alcohol VOCs by the nano-TiO_2/diatomite composite, the appropriate relative humidity for the degradation of the VOCs was related to the length of the carbon chain: the longer the carbon chain, the higher the appropriate relative humidity. The optimal relative humidity of acetone, MEK and 2-heptanone was 5%, 15%, and 30%, respectively. The optimal relative humidity for the degradation of isopropanol, isobutanol, and 1-heptanol was 5%, 15%, and 50%, respectively. The degradation still occurred when the relative humidity was 0 due to the superoxide radicals and hydroxyl radicals produced from oxygen and maybe the extremely low water vapor level. However, the degradation hardly occurred when the oxygen content was 0 due to the lack of radicals produced from the reaction of oxygen. Overall, the relative humidity and reaction atmosphere had different influences on the photocatalytic degradation of ketone and alcohol VOCs.

Conflicts of interest

There are no conflicts to declare.

Acknowledgements

The authors gratefully acknowledge the financial support provided by the National Key R&D Program of China (2017YFB0310803-4), the Young Elite Scientists Sponsorship Program by CAST (2017QNRC001), and the Fundamental Research Funds for the Central Universities (2015QH01 and 2010YH10). The first author thanks the China Scholarship Council (CSC) for financial support.

References

1 H. Dai, S. Jing, H. Wang, Y. Ma, L. Li, W. Song and H. Kan, *Sci. Total Environ.*, 2017, **577**, 73–83.
2 A. Steinemann, *Air Qual., Atmos. Health*, 2015, **8**, 273–281.
3 A. Krishnamurthy, B. Adebayo, T. Gelles, A. Rownaghi and F. Rezaei, *Catal. Today*, DOI: 10.1016/j.cattod.2019.05.069.
4 C. Yang, G. Miao, Y. Pi, Q. Xia, J. Wu, Z. Li and J. Xiao, *Chem. Eng. J.*, 2019, **370**, 1128–1153.
5 W. Zou, B. Gao, Y. S. Ok and L. Dong, *Chemosphere*, 2019, **218**, 845–859.
6 X. Du, Y. Wu, Y. Kou, J. Mu, Z. Yang, X. Hu and F. Teng, *J. Alloys Compd.*, 2019, **810**, 151917.
7 L. Mohan V, S. M. S. Nagendra and M. P. Maiya, *J. Environ. Chem. Eng.*, 2019, **7**, 103455.
8 H. Huang, G. Liu, Y. Zhan, Y. Xu, H. Lu, H. Huang, Q. Feng and M. Wu, *Catal. Today*, 2017, **281**, 649–655.
9 L. Wang, W. Wang, M. Liu, H. Ge, W. Zha, Y. Wei, E. Fei, Z. Zhang, J. Long, R. Sa, Y.-J. Wang, X. Fu and R. Yuan, *J. Catal.*, 2019, **377**, 322–331.
10 N. S. Kovalevskiy, M. N. Lyulyukin, D. S. Selishchev and D. V. Kozlov, *J. Hazard. Mater.*, 2018, **358**, 302–309.
11 C.-C. Wang, X.-H. Yi and P. Wang, *Appl. Catal., B*, 2019, **247**, 24–48.
12 L. Tang, Z.-Q. Lv, Y.-C. Xue, L. Xu, W.-H. Qiu, C.-M. Zheng, W.-Q. Chen and M.-H. Wu, *Chem. Eng. J.*, 2019, **374**, 975–982.
13 T.-D. Pham and B.-K. Lee, *J. Hazard. Mater.*, 2015, **300**, 493–503.
14 M. Li, B. Lu, Q.-F. Ke, Y.-J. Guo and Y.-P. Guo, *J. Hazard. Mater.*, 2017, **333**, 88–98.
15 J. Lyu, J. Gao, M. Zhang, Q. Fu, L. Sun, S. Hu, J. Zhong, S. Wang and J. Li, *Appl. Catal., B*, 2017, **202**, 664–670.
16 G. Zhang, Y. Liu, S. Zheng and Z. Hashisho, *J. Hazard. Mater.*, 2019, **364**, 317–324.
17 L. Deng, P. Yuan, D. Liu, F. Annabi-Bergaya, J. Zhou, F. Chen and Z. Liu, *Appl. Clay Sci.*, 2017, **143**, 184–191.

18 J. Zhu, P. Zhang, Y. Wang, K. Wen, X. Su, R. Zhu, H. He and Y. Xi, *Appl. Clay Sci.*, 2018, **159**, 60–67.
19 C. Li, Z. Sun, A. Song, X. Dong, S. Zheng and D. D. Dionysiou, *Appl. Catal., B*, 2018, **236**, 76–87.
20 R. Portela, I. Jansson, S. Suárez, M. Villarroel, B. Sánchez and P. Avila, *Chem. Eng. J.*, 2017, **310**(Part 2), 560–570.
21 A. Mishra, A. Mehta and S. Basu, *J. Environ. Chem. Eng.*, 2018, **6**, 6088–6107.
22 Y. Chen, Q. Wu, L. Liu, J. Wang and Y. Song, *Appl. Surf. Sci.*, 2019, **467–468**, 514–525.
23 Y. Chen and K. Liu, *Chem. Eng. J.*, 2016, **302**, 682–696.
24 C. Li, Z. Sun, R. Ma, Y. Xue and S. Zheng, *Microporous Mesoporous Mater.*, 2017, **243**, 281–290.
25 Z. Sun, C. Li, G. Yao and S. Zheng, *Mater. Des.*, 2016, **94**, 403–409.
26 G. Zhang, Z. Sun, Y. Duan, R. Ma and S. Zheng, *Appl. Surf. Sci.*, 2017, **412**, 105–112.
27 L. Zhong and F. Haghighat, *Build. Environ.*, 2018, **144**, 427–436.
28 O. Debono, V. Gaudion, N. Redon, N. Locoge and F. Thevenet, *Chem. Eng. J.*, 2018, **353**, 394–409.
29 M. Malayeri, F. Haghighat and C.-S. Lee, *Build. Environ.*, 2019, **154**, 309–323.
30 H. E. Whyte, C. Raillard, A. Subrenat and V. Héquet, *Chem. Eng. J.*, 2018, **352**, 441–449.
31 R. A. R. Monteiro, A. M. T. Silva, J. R. M. Ângelo, G. V. Silva, A. M. Mendes, R. A. R. Boaventura and V. J. P. Vilar, *J. Photochem. Photobiol., A*, 2015, **311**, 41–52.
32 M. Tong, S. Yuan, S. Ma, M. Jin, D. Liu, D. Cheng, X. Liu, Y. Gan and Y. Wang, *Environ. Sci. Technol.*, 2016, **50**, 214–221.
33 V. Augugliaro, M. Bellardita, V. Loddo, G. Palmisano, L. Palmisano and S. Yurdakal, *J. Photochem. Photobiol., C*, 2012, **13**, 224–245.
34 J. Mo, Y. Zhang and Q. Xu, *Appl. Catal., B*, 2013, **132–133**, 212–218.
35 M. Sleiman, P. Conchon, C. Ferronato and J.-M. Chovelon, *Appl. Catal., B*, 2009, **86**, 159–165.
36 E. J. Park, H. O. Seo and Y. D. Kim, *Catal. Today*, 2017, **295**, 3–13.
37 P. Pichat, *Appl. Catal., B*, 2010, **99**, 428–434.
38 A. H. Mamaghani, F. Haghighat and C.-S. Lee, *Appl. Catal., B*, 2019, **251**, 1–16.
39 J. Zhang, Y. Hu, X. Jiang, S. Chen, S. Meng and X. Fu, *J. Hazard. Mater.*, 2014, **280**, 713–722.
40 W. Li, D. Li, Y. Lin, P. Wang, W. Chen, X. Fu and Y. Shao, *J. Phys. Chem. C*, 2012, **116**, 3552–3560.
41 Y. Nosaka and A. Y. Nosaka, *Chem. Rev.*, 2017, **117**, 11302–11336.

